Journal of Structural Geology, Vol. 10, No. 7, pp. 755 to 763, 1988
Printed in Great Britain

0191-8141/88 $03.00 + 0.00

Vorticity and strain analysis using Mohr diagrams

CEES W. PASSCHIER and JANOS L. URAI

Instituut voor Aardwetenschappen, P.O. Box 80021, 3508TA, Utrecht, The Netherlands

(*Received* 16 *December* 1987; *accepted in revised form* 9 *May* 1988)

Abstract—Fabric elements in naturally deformed rocks are usually of a highly variable nature, and measurements contain a high degree of uncertainty. Calculation of general deformation parameters such as finite strain, volume change or the vorticity number of the flow can be difficult with such data. We present an application of the Mohr diagram for stretch which can be used with poorly constrained data on stretch and rotation of lines to construct the best fit to the position gradient tensor; this tensor describes all deformation parameters. The method has been tested on a slate specimen, yielding a kinematic vorticity number of 0.8 ± 0.1.

INTRODUCTION

ONE of the aims in structural geology is the reconstruction of finite deformation parameters and the deformation history for small volumes of rock from the geometry and orientation of fabric elements. Such data can then be used for reconstruction of large-scale deformation patterns and eventually in tracing regional tectonics. Methods for determination of the two finite deformation parameters, finite strain and volume change, are well established (see e.g. Gratier 1983, Ramsay & Huber 1983) but deformation history is not so easily reconstructed: every progressive step of the deformation overprints older effects, and all data must be retrieved from the final rock fabric.

At present there are two ways to increase our capability to obtain data on the deformation path from the final fabric: (i) determination of the mechanisms of fabric development in order to correctly interpret those fabrics in terms of flow or deformation parameters (e.g. Platt & Vissers 1980, Lister & Snoke 1983, Jessell 1986, Passchier & Simpson 1986, Schmid & Casey 1986); and (ii), development of a theoretical background showing how the variation of flow parameters with time influences finite deformation (Means *et al.* 1980, De Paor 1983, Passchier 1986, in press).

One of the most important parameters to determine the shape of the deformation path is the kinematic vorticity number. This number can be somewhat loosely described as the ratio of pure shear to simple shear components of flow (for definition, see Truesdell 1954 and Means *et al.* 1980). The value of this number during deformation has important consequences for the stretch and rotation history of individual material lines. For example, if flow in two shear zones was characterized by different vorticity numbers, the deformation history in shear zone and wall rock of both zones must have been different for each, even though finite strain and volume change values may be identical. Therefore, knowledge of the vorticity number is useful in structural analysis, especially for the study of crystallographic fabric development and in regional tectonic reconstructions.

Two recent papers have suggested ways to determine this number in naturally deformed rocks (Ghosh 1987, Passchier 1988). These methods rely on the recognition that certain fabric elements in naturally deformed rocks have a memory for sense of shear and flow vorticity number. Some examples are rotated porphyroblast–foliation systems (Ghosh 1987); sets of folded and boudinaged veins; sets of rigid objects of variable aspect ratio; tails of recrystallized material around rigid objects; and systems of bedding, foliation and syn-kinematic fibrous veins (Passchier 1988).

FLOW PARAMETERS AND DEFORMATION

Homogeneous ductile flow can be geometrically described by equations such as

$$\dot{X} = \mathbf{L}X,$$

where $\mathbf{L}$ is the velocity gradient tensor, X a position in space and $\dot{X}$ the rate of displacement of a particle at that position (Malvern 1969, Lister & Williams 1983, Passchier 1986). Even where bulk flow is not homogeneous, the deforming volume can be subdivided into approximately homogeneously deforming parts for which equations as given above are a satisfactory approximation. $\boldsymbol{L}$ can be described in terms of a mean stretching rate, r, a volume change rate, a, and a kinematic vorticity number

$$W_n = W/2r,$$

where W is the flow vorticity (Means *et al.* 1980, Passchier 1986). Note that for simple shear flow $W_n = 1$ and for pure shear flow $W_n = 0$.

Finite deformation produced by ductile flow can be described by the Lagrangian position gradient tensor $\boldsymbol{F}$ which relates the position of material particles in the undeformed and deformed states as

$$X' = \boldsymbol{F}X.$$

$\boldsymbol{F}$ contains information on finite strain, volume change and rigid body rotation. For suitably chosen reference

frames (as explained below), a simple relationship exists between components of F and W_n (Passchier in press). In practice, however, it is difficult to calculate F from fabric data in naturally deformed rocks, or even to determine which and how many fabric data are needed for a solution. A Mohr circle construction can solve most of these problems and can also be used to calculate W_n from components of F.

THE MOHR CIRCLE FOR F

Finite deformation produced by flow types of monoclinic or higher symmetry can be defined by a 3 × 3 tensor F, or by a two-dimensional 2 × 2 tensor describing flow in planes normal to the vorticity vector, and a factor describing stretch parallel to this vector. Means (1983) explained how any 2 × 2 tensor (such as F) can be represented by a Mohr circle. This is done using the components F_{ij} of the tensor to define two points in Mohr space with Cartesian co-ordinates (F_{22}, F_{12}) and (F_{11}, $-F_{21}$). These points lie at opposite ends of a Mohr circle diameter (Fig. 1a). In fact, Cartesian co-ordinates of any two points 180° apart on a Mohr circle give the numerical components of the tensor with respect to a specific set of co-ordinate axes. This is the Mohr circle equivalent of the tensor transformation equation (see Means *et al.* 1980 for full explanation and proof).

In the case of the position gradient tensor, Means (1982) has elegantly shown that the *polar* co-ordinates of points on the Mohr circle have interesting properties. They are equal to stretch (s) and angle of rotation of material lines after a given finite strain (Fig. 1b–d). In addition, the angle (2η) measured between points *along* the circle is equal to twice the angle between these lines (in real space) in the undeformed state.

Progressive deformation is described in this Mohr diagram by a series of circles 'growing' in a regular way from (1,0), depending on the degree of non-coaxiality (see Passchier 1988 and in press for further explanation). The off-axis position of these Mohr circles reflects the rigid body rotation component of F. For homogeneous flow, Passchier (1988, in press) has presented the relationship

$$Q/R = W_n^m,$$

where Q is the elevation of the circle centre above the horizontal axis, R is the circle radius (Fig. 1d) and W_n^m is a mean value of the kinematic vorticity number for the local deformation history, which equals W_n in the special case that this number remained constant during the deformation. Note that this equation is only valid if F is described in a reference frame which is fixed with respect to the instantaneous stretching axes (ISA) of the flow (Lister & Williams 1983, Passchier 1986). These are the orthogonal directions of minimum and maximum stretching rate in a homogeneously deforming material. Although ISA cannot be directly represented in a Mohr diagram for F, *material lines* coinciding with ISA at the first increment of deformation can be shown to lie at opposite ends of a horizontal diameter of the circle and be used as useful markers (see e.g. C and D in Fig. 5).

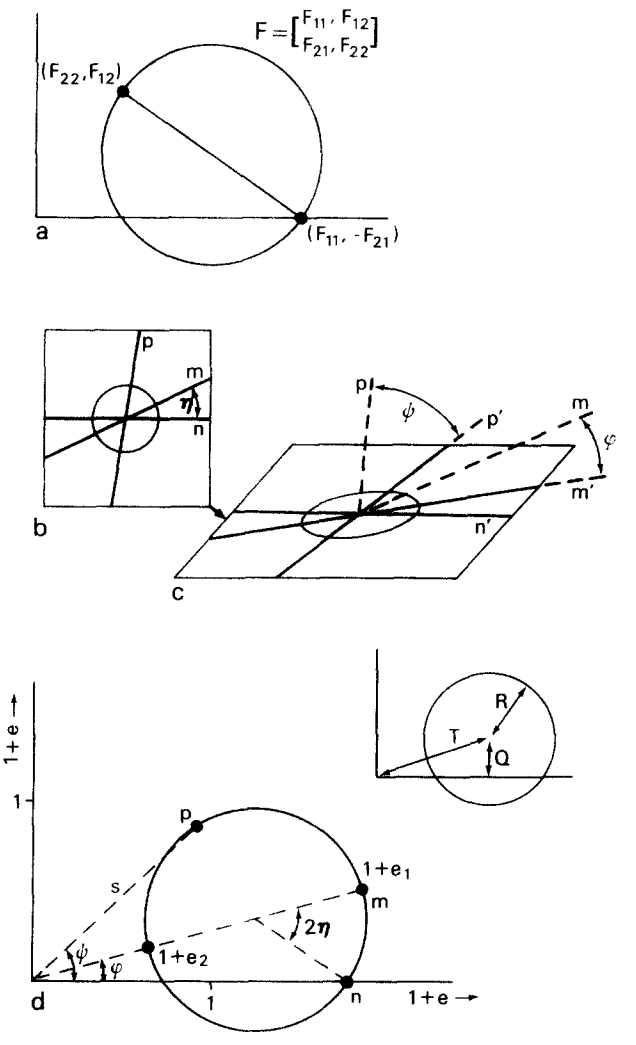

Fig. 1. (a) Representation of a tensor F in Mohr space using the convention of Means *et al.* (1980). Homogeneous deformation in real space (b) and (c) can be represented as a Mohr circle (d) by plotting stretch and rotation of individual material lines (p, m, n) as polar co-ordinates in Mohr space (e.g. s, ψ for line p). The angle η between any two lines (e.g. m and n) in true space before deformation is plotted as 2η along the Mohr circle. Size and position of the Mohr circle depends on the deformation parameters and can be defined by the numbers T, Q and R.

In what follows, we present a method to reconstruct the Mohr diagram for F using data on stretch and rotation of lines with respect to ISA and on area change in the plane normal to the vorticity vector. The Mohr diagram is then used to calculate F, W_n^m and other deformation parameters.

DATA AND INTERPRETATION

The samples investigated in this study were taken from a slate quarry on the north side of Highway No. 4, New York state, 3 km SW from the New York–Vermont border. The regional geological setting is in an internally folded thrust slice, bounded by melanges of the Taconic thrust system (see Bosworth & Kidd 1985 and fig. 12 of

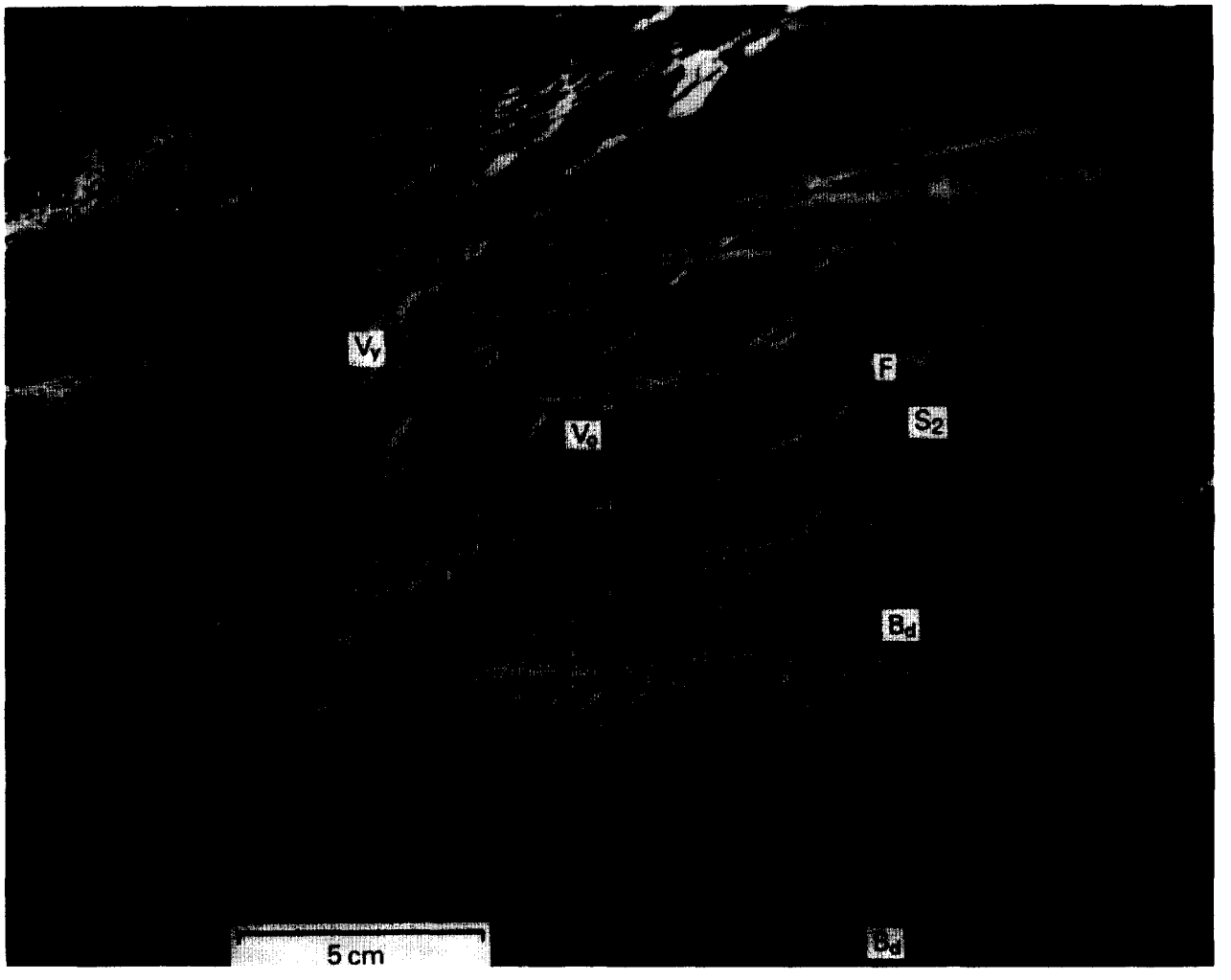

Fig. 2. Photograph of the outcrop studied, looking south. B_d—bedding with refracted veins; *F*—folded bedding associated with veins in the closure; V_0 and V_y—calcite veins; S_2—main foliation.

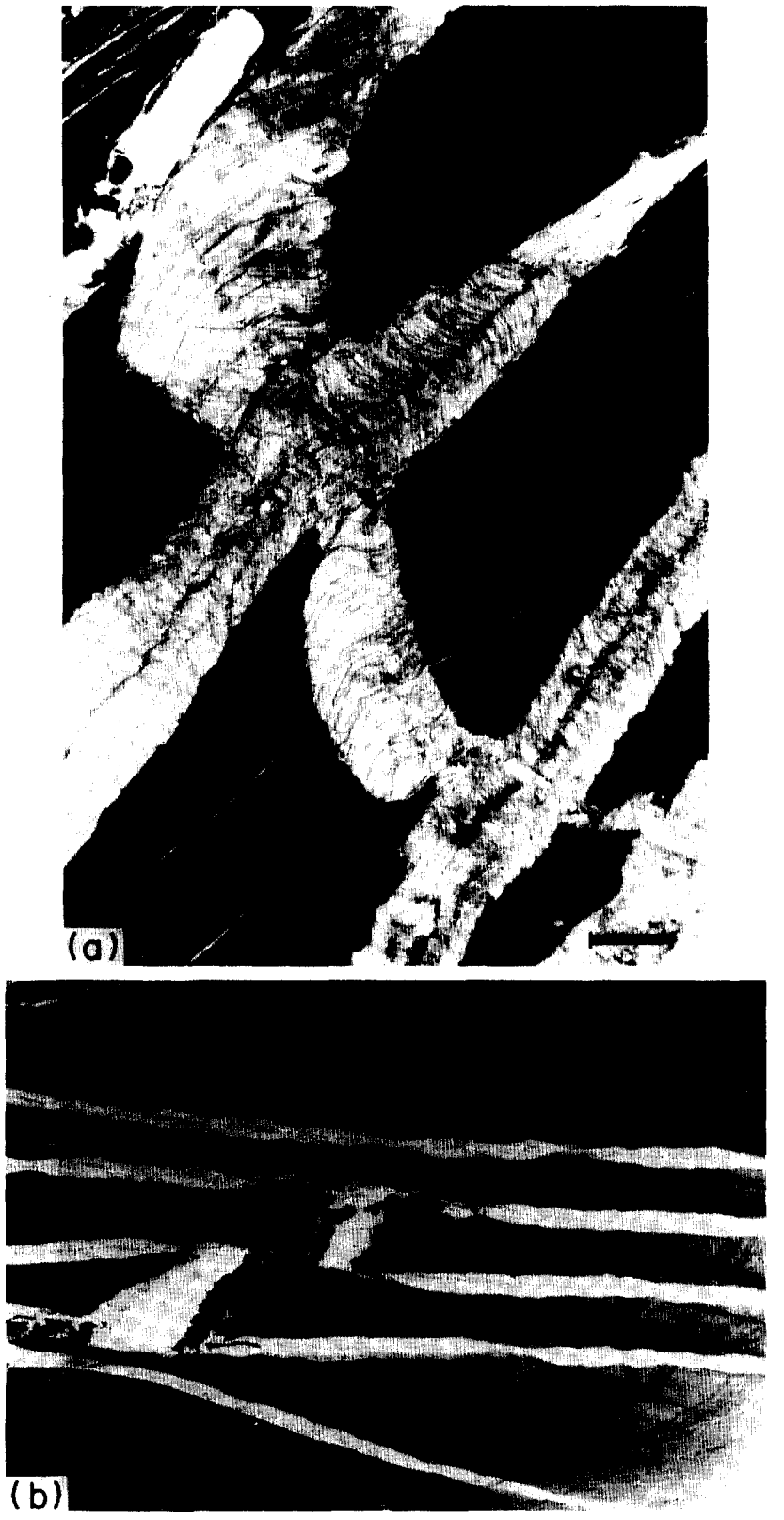

Fig. 3. (a) Photomicrograph of V_0–V_y intersection showing fibres in boudin necks in V_0, parallel to fibres in V_y. The penetrative cleavage in the slate is S_2. Scale of bar is 0.1 mm. (b) Photograph of the thin section on which the microprobe measurements in Fig. 7 were carried out. Traverses are indicated by black lines, scale bar is 5 mm.

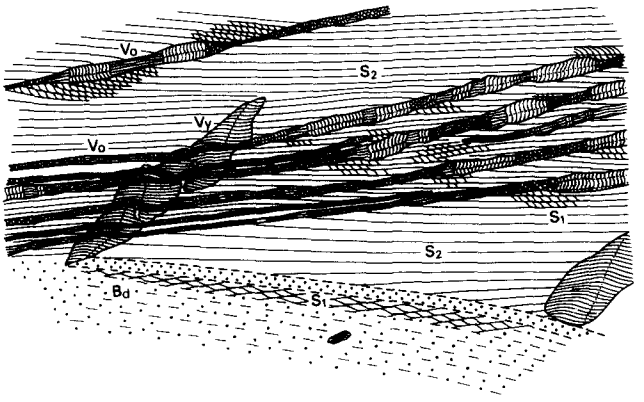

Fig. 4. Tracing of a photograph of a thin section (width 20 mm), showing the fabric elements used in this study. B_d—bedding; S_1 and S_2—cleavages; V_0 and V_y—two generations of antitaxial fibrous veins. The internal structure of the veins was drawn to indicate grain shapes, and lines do not always correspond to fibre boundaries. Pyrite crystals (black) are associated with quartz fibres in pressure fringes.

Bosworth & Vollmer 1981 for an illustration of the large-scale structure). From the map of Bosworth & Kidd (1985), it is apparent that the quarry is located on the normal limb of a west-facing, tight to isoclinal, moderately eastward-inclined syncline–anticline pair and our interpretation of the small-scale deformation is in agreement with this setting.

In sections perpendicular to bedding and intersection lineations, the following fabric elements are present (Figs. 2 and 4).

(a) Layers of black slate (B_d), up to 5 cm thick, composed of white mica, chlorite, quartz and pyrite + other opaques, alternating with sandy layers rich in quartz, calcite and pyrite.

(b) A first cleavage (S_1) parallel to bedding, which is developed as a continuous cleavage in the slate layers and as a spaced, pressure solution type cleavage in the sandy layers.

(c) Local small-scale asymmetric folds of bedding and S_1, spatially associated with calcite veins (see Figs. 2 and 4).

(d) A second cleavage S_2, developed at low angle to bedding, completely transposing S_1, which is only preserved in hinges of the folds just described. Regions with S_2 development show a marked concentration of opaque particles, and a decrease in quartz and calcite content.

(e) Two generations (V_0 followed by V_y) of fibrous antitaxial calcite veins, with a well-defined median line (Durney & Ramsay 1973), mostly present in the slate layers. On entering a quartz-rich layer from the slate, they are commonly strongly refracted (Fig. 2). Veins from set V_0 often occur along the axial plane of the folds, approximately perpendicular to the local orientation of S_1. They are strongly boudinaged, with vein-parallel calcite fibres growing in the boudin-necks (Fig. 3a). The original fibrous texture is surprisingly well preserved, however, with the internal microstructure of calcite fibres ranging from optically completely strain-free to slightly deformed, with incipient recrystallization along the grain boundaries.

Veins from set V_y show clear cross-cutting relationships with S_2, and the curved calcite fibres are invariably almost completely strain-free optically, with minor twinning. V_y fibres adjacent to the vein wall are parallel to fibres in the boudin-necks of V_0 and to terminations of pressure fringes around pyrite framboids in the slate (Figs. 3a and 4). Serial sectioning shows the lines of intersection of bedding, cleavage, and both sets of veins to be parallel to the fold axes. We therefore infer this intersection to be parallel to the vorticity vector of flow in the volume of slate considered. No traces of stretching of V_0 in this direction could be detected, which means that possible bulk volume change equals area change in the surface normal to the vorticity vector.

We interpret the data in terms of a deformation history as follows. After the formation of the first cleavage (which represents an unknown deformation stage), the material deformed in a strongly non-coaxial way. At some time during this stage, the first set of veins (V_0) was formed at a high angle to bedding, approximately in a tension gash orientation (Ramsay & Huber 1983, p. 50). Williams and Urai (in press) show that antitaxial fibres in veins do not necessarily track the opening direction of such veins. In the rocks studied, however, undeformed fibres in V_0 invariably connect marker layers over the veins, indicating that here fibres grew parallel to the opening direction, and therefore to ISA (Durney & Ramsay 1973, Williams & Urai in press). The veins rotated clockwise (looking south), causing a perturbation of the flow pattern and subsequent generation of the folds (e.g. Hudleston 1984). Deformation was strongly partitioned between the more competent quartz-rich layers and the slate, causing the observed refraction of the veins (Lister & Williams 1983). After initial shortening, the veins entered the extension field and were boudinaged and broken, with calcite fibres growing in the boudin-necks. During rotation of V_0 part of the fibres were plastically deformed and therefore could have changed their orientation with respect to the vein walls; however the deformed fibres are parallel to fibres in undeformed V_0 veins, so this was probably not a significant effect. According to Bosworth & Vollmer (1981), deformation took place under low temperature, high fluid pressure conditions. Calcite was apparently stronger than the matrix and deformed dominantly in a brittle way. V_y was formed at a later stage, and these veins rotated over approximately 45° until the end of deformation.

Because of the straight S_2 cleavage and the absence of large systematic changes in the angle between fabric elements in these regions it seems reasonable to assume that homogeneous deformation was approached in the slate layers (Fig. 2).

RECONSTRUCTION

Instead of plotting data on stretch and rotation of material lines (Fig. 5a) as polar co-ordinates in an orthogonal reference frame to find the diameter and

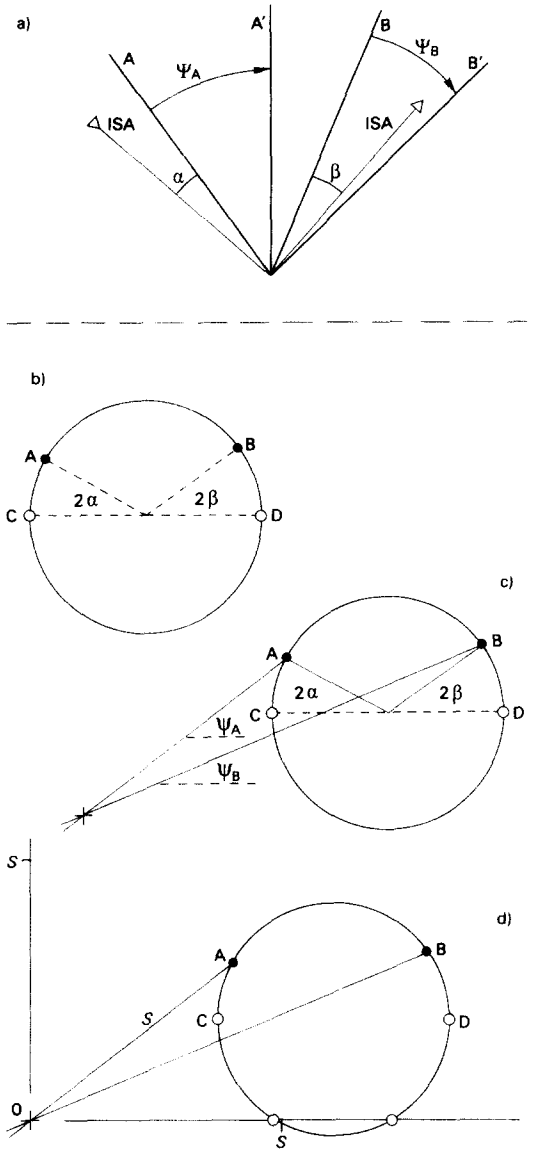

Fig. 5. Construction method of the Mohr diagram for F. Data on initial orientation of two material lines A and B with respect to C and D (α and β) in real space (a) can be plotted in Mohr space on an arbitrarily chosen circle (b) as double angles. Material lines C and D coincided with ISA at the onset of deformation. The reorientation of A and B due to finite deformation (ψ_A,ψ_B) in true space (a) can be plotted in Mohr space (b) by drawing lines from A and B at angles ψ_A and ψ_B to a marker line (|| to C–D) into Mohr space. Their intersection represents the origin of the reference frame of Mohr space. The dimensions on the co-ordinate axes can be found (d) if the stretch (s) on one of the material lines (A in this case) is known.

position of the Mohr circle (Allison 1984, De Paor & Means 1984, Treagus 1986), we propose to use the following construction: starting with a circle of arbitrary diameter (Fig. 5b), data on stretch and rotation of material lines are used to find the origin and dimensions of the Mohr space reference frame (Fig. 5c & d). Finite deformation parameters and W_n^m can then be read from the Mohr circle (Fig. 5d). This method has the advantage that uncertainties in stretch and rotation values can easily be incorporated in the construction to find the limits of uncertainty of the results.

For the rock studied, we proceed as follows:

(i) the calcite fibres indicate that V_0 was initially oriented at 0–10° from the instantaneous shortening axis, and rotated over 86–96° with respect to this axis (Fig. 6a);

(ii) assuming only minor shear strain in the sandy layers (i.e. no significant rotation of V_0 with respect to B_d in these; Lister & Williams 1983), and that V_0 veins were straight at the time of their formation, the angle between V_0 and B_d before deformation can be constrained at 90–120° (Fig. 6a);

(iii) from the angle of refraction we deduce a rotation of 71–104° between V_0 and B_d. We start the construction with an arbitrary circle, reference line and two points which represent the material lines coinciding with ISA at the onset of deformation (C and D in Fig. 5): these are chosen on the diameter of the circle which is parallel to the reference line. The ranges of possible orientations of V_0 and B_d with respect to ISA now define segments along the circle as shown in Fig. 6(c). In the diagram, the angle of rotation of V_0 or B_d with respect to the external reference frame can be plotted as lines radiating from the respective positions on the circle (Fig. 6c). The origin of the co-ordinate system necessarily lies somewhere along such a line. Intersecting lines from different data points, such as old veins and bedding, can determine this position accurately; Fig. 6(c) shows how they define, within their range of uncertainty (Fig. 6a), a small domain which must contain the origin of the Mohr space. The dimensions of the diagram can now be determined as follows. The length of the lines joining possible V_0 positions on the Mohr circle with the domain containing the origin of Mohr space (Fig. 6b & c) equals the stretch of these lines in real space. A stretch value is estimated using the relative length of boudinaged parts of V_0 and their boudin necks in veins which preserved their original fibrous habit; in these veins, the assumption of completely brittle behaviour during stretching seems reasonable. We have made a correction for the inferred value of initial shortening before boudinage started. By this method, s was relatively poorly constrained at 1.25 ± 0.4 (Fig. 6b).

AREA CHANGE MEASUREMENTS

Area change during the studied part of the deformation in the plane for which F is described, was estimated by means of a chemical analysis. Changes in bulk composition were measured using a microprobe with a defocused beam (spot diameter 100 μm), along traverses parallel to well-defined bedding traces in small-scale folds. The analysis was done in a different hand specimen from the same outcrop, where S_2 in the slate was locally less intensely developed (Fig. 3b), allowing the transition to a penetratively developed S_2 to be followed along bedding. The results show a clear trend: going from hinge to limb (i.e. with increasing intensity of S_2 development) there is a clear increase in concentration of elements like Al_2O_3 and TiO_2 (Fig. 7), together with a decrease in SiO_2 and CaO. Using the techniques described by Gratier (1983), an area decrease ΔA of

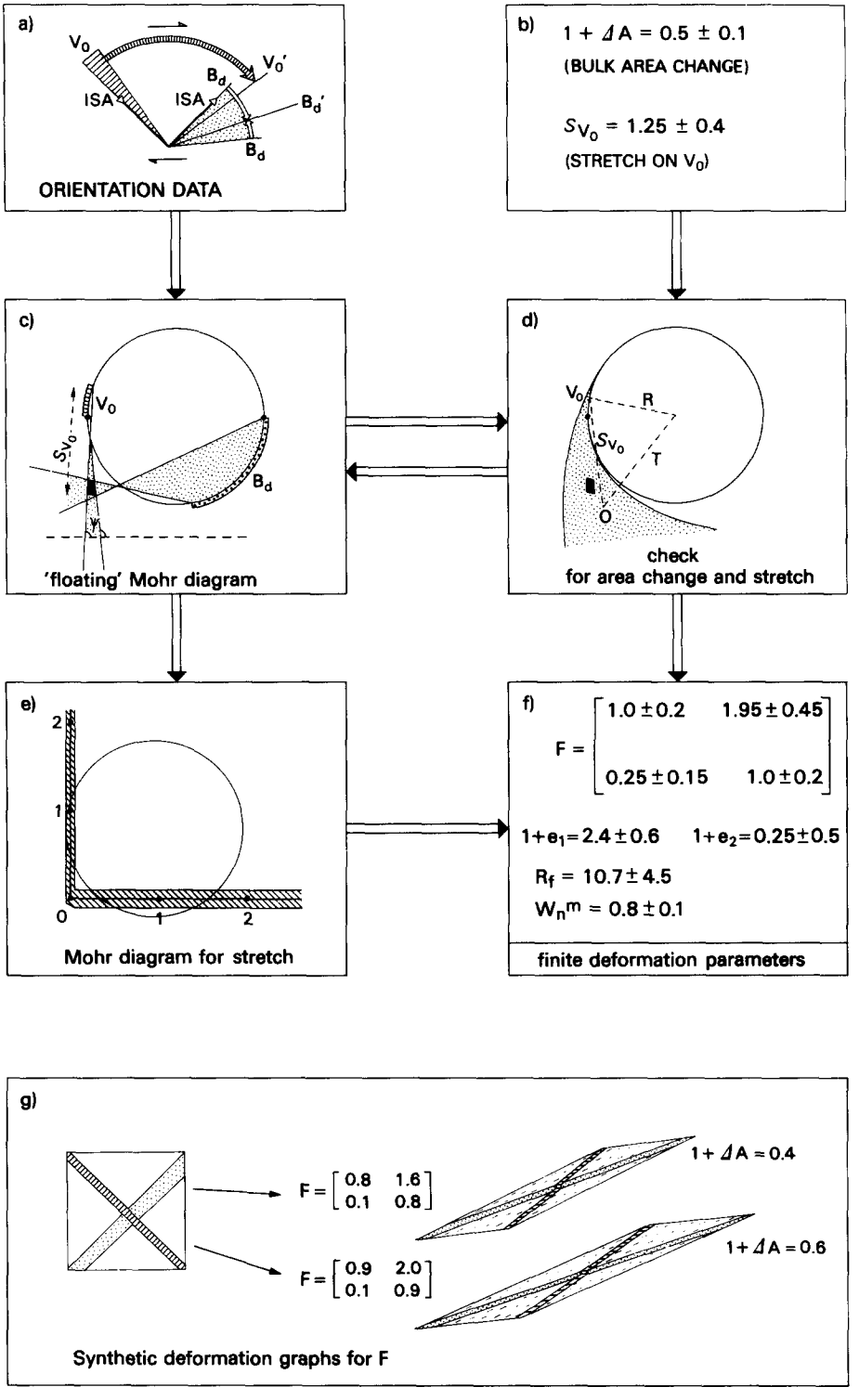

Fig. 6. (a) Data on original position and rotation of old veins (V_0) and bedding (B_d) with respect to ISA in real space. Striped and stippled domains show range of uncertainty of orientation of V_0 and B_d, respectively. (b) Data on bulk area change and stretch on V_0. (c) Orientation data define the two stippled domains in Mohr space which must contain the origin; their intersection (black) gives the range of uncertainty in the position of the origin for the data in (a). (d) Combined data on ΔA and stretch of V_0 define the stippled domain which must contain the origin; these results agree with those in (c). R and T are defined in Fig. 1(d). (e) The Mohr diagram for F, based on (c) and (d). Ornamented domain indicates the range of uncertainty in the position of the reference frame. (f) Finite deformation parameters as determined from (e) and (d). (g) Synthetic deformation graphs for two tensors within the range of uncertainty of F. Stippled: B_d, striped: V_0.

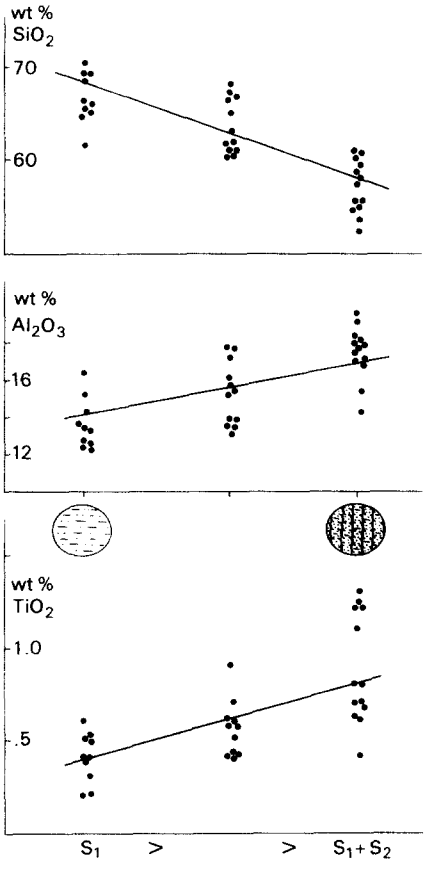

Fig. 7. Data from microprobe measurements showing change in chemical composition associated with development of S_2 in the sample of Fig. 3(b).

approximately 50 ± 10% is calculated, assuming no area change in the hinge regions (this is suggested by the absence of overgrowth structures in these regions), and unit stretch in the direction parallel to the vorticity vector. Calculations based on the enrichment of opaques (assumed to be immobile) in these zones are in agreement with this number. The microstructure in the sample for which a Mohr circle was constructed is identical to that in the most intensely cleaved part of the sample in which area change was measured. We therefore assume that area change in both samples is of similar magnitude.

One of the properties of the Mohr circle for $\boldsymbol{F}$ is the relationship (table 1 in Passchier in press):

$$T^2 = 1 + R^2 + \Delta A \text{ (Fig. 1d)}.$$

In a dimensionless Mohr diagram, the origin must lie at distance T from the circle centre and at distance s (representing the stretch of V_0), from the position of old veins on the edge of the circle. R has a fixed length in a dimensionless Mohr diagram, but its magnitude depends on the chosen scale. Varying the scale of the diagram allows the construction of a domain which must contain the origin of the Mohr space for specific values of s and ΔA (Fig. 6d). The domain in Mohr space, constructed in the previous paragraph from the rotation of old veins and bedding, lies within the curves of Fig. 6(d) for the range of uncertainty of the initial orientation of old veins. This supports the viability of the construction method.

Note here that the tensor $\boldsymbol{F}$ reconstructed in this way describes only part of the total deformation, from the point in time when V_0 was formed.

DISCUSSION AND CONCLUSIONS

The diagram constructed in Fig. 6(e) shows the range within which the reference frame of the Mohr diagram must lie. Using the conventions of Fig. 1(a) (Means 1983), this allows direct reconstruction of the components of $\boldsymbol{F}$ (including their range of uncertainty) and calculation of other deformation parameters (Fig. 6f) as follows.

(1) The 'mean' kinematic vorticity number W_n^m, calculated from the Q/R ratio (Passchier in press and in preparation), is estimated at 0.8 ± 0.1; i.e. flow was non-coaxial approaching simple shear, but had a pure shear component.

(2) Finite strain $(1 + e)$ values, measured as maximum and minimum stretch values on the circle in Fig. 5(d) are 0.25 ± 0.5 and 2.4 ± 0.6.

(3) Stretch of the bedding is between 1.2 and 2.1 depending on its original orientation with respect to V_0, but always exceeding that of V_0. Such high stretch values are not obvious from the microstructure in the bedding, but are confirmed by boudinage of thick beds elsewhere in the outcrop (Fig. 2), and by fringes around pyrite grains.

The effect of the deformation described by $\boldsymbol{F}$ is illustrated in 'synthetic deformation graphs' (Fig. 6g) for $\boldsymbol{F}$, based on Fig. 6(e); they have been constructed reading stretch and rotation for sides of a square from two opposite points in the Mohr circle.

(4) Folding of bedding occurs during extension and is a consequence of flow partitioning around the veins.

In conclusion, a Mohr diagram for $\boldsymbol{F}$ can be constructed from relatively poorly constrained data of variable nature. These properties make the method useful for the analysis of naturally deformed rocks, in which control on the nature of available data is poor and data can have a large range of uncertainty. The effect of each uncertainty in the data can be followed in the Mohr diagram and weighted in final conclusions or further work.

Acknowledgements—We wish to thank Win Means for introducing J. L. Urai to the outcrop studied, for enjoyable discussions on vein fibres and for valuable suggestions on the manuscript. We are grateful to Manfred van Bergen for help with the (NWO/WACOM supported) microprobe. Thorough reviews by Declan De Paor and Sue Treagus are gratefully acknowledged. We thank the RSES of ANU for all their hospitality, to J. L. Urai during a visiting fellowship and to C. W. Passchier during his stay in Canberra awaiting the consequences of the grounding of Nella Dan. This work was supported by a C&C Huygens fellowship from the Netherlands Organization for the Advancement of Pure Research (NWO) and by NSF grant EAR 8306166 to J. L. Urai.

REFERENCES

Allison, I. 1984. The pole of the Mohr diagram. *J. Struct. Geol.* **6**, 331–333.

Bosworth, W. & Kidd, W. S. F. 1985. Thrusts, melanges, folded

thrusts and duplexes in the Taconic foreland. In: *New York State Geological Association 57th Annual Meeting Field Trip Guidebook* (edited by Lindemann, R.). Skidmore College, Saratoga, New York.

Bosworth, W. & Vollmer, F. W. 1981. Structures of the medial Ordovician flysch of Eastern New York: deformation of synorogenic deposits in an overthrust environment. *J. Geol.* **89**, 551–568.

De Paor, D. G. 1981. Unpublished Ph.D. Thesis, National University of Ireland.

De Paor, D. G. 1983. Orthographic analysis of geological structures 1. Deformation theory. *J. Struct. Geol.* **5**, 255–277.

De Paor, D. G. & Means, W. D. 1984. Mohr circles of the first and second kind and their use to represent tensor operations. *J. Struct. Geol.* **6**, 693–701.

Durney, D. W. & Ramsay, J. G. 1973. Incremental strains measured by syntectonic crystal growths. In: *Gravity and Tectonics* (edited by De Jong, K. A. & Scholten, R.). John Wiley, New York, 67–96.

Ghosh, S. K. 1987. Measure of non-coaxiality. *J. Struct. Geol.* **9**, 111–115.

Gratier, J. P. 1983. Estimation of volume changes by comparative chemical analyses in heterogeneously deformed rocks (folds with mass transfer). *J. Struct. Geol.* **5**, 329–339.

Hudleston, P. J. 1984. Generation of folds in shear zones. *Geol. Soc. Am. Abs. w. Prog.* **16**, 546.

Jessell, M. V. 1986. Grain boundary migration and fabric development in experimentally deformed octachloropropane. *J. Struct. Geol.* **8**, 527–542.

Lister, G. S. & Snoke, A. 1983. *S–C* mylonites. *J. Struct. Geol.* **6**, 617–638.

Lister, G. S. & Williams, P. F. 1983. The partitioning of deformation in flowing rock masses. *Tectonophysics* **92**, 1–33.

Malvern, L. E. 1969. *Introduction to the Mechanics of a Continuous Medium.* Prentice Hall, Englewood Cliffs, New Jersey.

Means, W. D. 1982. An unfamiliar Mohr circle construction for finite strain. *Tectonophysics* **80**, T1–T6.

Means, W. D. 1983. Application of the Mohr-circle construction to problems of inhomogeneous deformation. *J. Struct. Geol.* **5**, 279–286.

Means, W. D., Hobbs, B. E., Lister, G. S. & Williams, P. F. 1980. Vorticity and non-coaxiality in progressive deformations. *J. Struct. Geol.* **2**, 371–378.

Passchier, C. W. 1986. Flow in natural shear zones—the consequences of spinning flow regimes. *Earth Planet. Sci. Lett.* **77**, 70–80.

Passchier, C. W. 1988. Flow path analysis in shear zones. *Geol. Rdsch.* **71**, 309–318.

Passchier, C. W. In press. The use of Mohr circles to describe non-coaxial flow regimes and resulting deformation in rocks. *Tectonophysics.*

Passchier, C. W. & Simpson, C. 1986. Porphyroclast systems as kinematic indicators. *J. Struct. Geol.* **8**, 831–843.

Platt, J. P. & Vissers, R. L. M. 1980. Extensional structures in anisotopic rocks. *J. Struct. Geol.* **2**, 397–410.

Ramsay, J. F. & Huber, M. I. 1983. *The Techniques of Modern Structural Geology, Vol. 1, Strain Analysis.* Academic Press, New York.

Schmid, S. M. & Casey, M. 1986. Complete fabric analysis of some commonly observed quartz *C*-axis patterns In: *Mineral and Rock Deformation; Laboratory Studies—The Paterson Volume* (edited by Hobbs, B. E. & Heard, H. C). *AGU Geophys. Monogr.* **36**, 263–295.

Treagus, S. H. 1986. Some applications of the Mohr diagram for three-dimensional strain. *J. Struct. Geol.* **8**, 819–830.

Truesdell, C. 1954. *The Kinematics of Vorticity.* Indiana University Press, Bloomington.

Williams, P. F. & Urai, J. L. In press. Curved vein fibres, an alternative explanation. *Tectonophysics.*